

# The growth of luminous red galaxies by merging

Morad Masjedi<sup>1</sup>, David W. Hogg<sup>1,2</sup>, Michael R. Blanton<sup>1</sup>

## ABSTRACT

We study the role of major and minor mergers in the mass growth of luminous red galaxies. We present small-scale ( $0.01 < r < 8 h^{-1} \text{Mpc}$ ) projected cross-correlation functions of 23043 luminous early-type galaxies from the Sloan Digital Sky Survey (SDSS) Luminous Red Galaxy (LRG) sample ( $0.16 < z < 0.30$ ,  $[M_{0.3i} - 5 \log_{10} h] \approx -22.75 \text{ mag}$ ) with all their companions in the SDSS imaging sample, split into color and luminosity subsamples with  $[M_{0.3i} - 5 \log_{10} h] < -18 \text{ mag}$ . We de-project the two-dimensional functions to obtain three-dimensional real-space LRG–galaxy cross-correlation functions for each companion subsample. We find that the cross-correlation functions are not purely power-law and that there is a clear “one-halo” to “two-halo” transition near  $1 h^{-1} \text{Mpc}$ . We convert these results into close pair statistics and estimate the LRG accretion rate from each companion galaxy subsample using timescales from dynamical friction arguments for each subsample of the companions. We find that the accretion onto LRGs is dominated by dry mergers of galaxies more luminous than  $L^*$ . We integrate the luminosity accretion rate from mergers over all companion galaxy subsamples and find that LRGs are growing by  $[1.7 \pm 0.1]$  percent per Gyr, on average, from merger activity at redshift  $z \sim 0.25$ . This rate is almost certainly an over-estimate because we have assumed that all close pairs are merging as quickly as dynamical friction allows; nonetheless it is on the low side of the panoply of measurements in the literature, and lower than any rate predicted from theory.

*Subject headings:* galaxies: elliptical and lenticular, cD — galaxies: evolution — galaxies: interactions — large-scale structure of universe — methods: statistical

---

<sup>1</sup> Center for Cosmology and Particle Physics, Department of Physics, New York University, 4 Washington Pl, New York, NY 10003

<sup>2</sup> To whom correspondence should be addressed: david.hogg@nyu.edu

## 1. Introduction

In the current paradigm for galaxy formation, the massive dark-matter halos in which galaxies reside have assembled throughout cosmic time by accretion and merging of smaller parts. There remains, however, substantial uncertainty about the formation and evolution of the galaxies in those halos, and the evolution of the stars and gas that compose them. A particularly important galaxy subpopulation in this research context is the luminous end of the red sequence of galaxies — consisting of concentrated, smooth, and typically elliptical galaxies that preferentially live in the densest regions of the Universe (Sandage 1972; Schneider et al. 1983; Roberts & Haynes 1994; Postman & Lauer 1995; Blanton et al. 2003b). Such galaxies account for a large fraction of the total stellar mass in the Universe (Hogg et al. 2002b; Rudnick et al. 2006; Brown et al. 2007), and thus understanding their formation is critical to understanding galaxy formation in general. This red sequence is clearly separated from the blue sequence of galaxies, which are typically lower in mass, more star-forming, gas-rich, morphologically “spiral,” and preferentially populate isolated regions (Strateva et al. 2001; Blanton et al. 2003b; Baldry et al. 2004; Balogh et al. 2004).

With uniform spectra, deep absorption lines, highly clustered distribution (“bias” around 2), and high luminosities (absolute magnitudes around  $-23$  mag), the Luminous Red Galaxies (LRGs) are excellent tracers of the density field on large scales (Eisenstein et al. 2001). For this reason, surveys of LRGs were the first to conclusively demonstrate the homogeneity of the Universe at low redshifts (Hogg et al. 2005) and to detect the baryon acoustic oscillation feature in the correlation function (Eisenstein et al. 2005). Their continuing importance to understanding fundamental cosmology underlines the need to better understand their nature.

Because luminous red galaxies are typically supported by velocity dispersion and not orderly rotation, it has been hypothesized that they form from mergers of two or more smaller galaxies (Toomre 1977). Such mergers have been shown in numerical simulations to produce disordered and velocity dispersion supported systems not unlike observed ellipticals (Negroponte & White 1983; Barnes & Hernquist 1996; Naab & Burkert 2003; Cox et al. 2006). In addition to such “major” mergers, LRGs could in principle grow over time from an accumulation of smaller mergers. If at least one of the merging galaxies is gas-rich, it often shows a large star-formation rate (Barton et al. 2000; Lambas et al. 2003; Nikolic et al. 2004; Smith et al. 2007), and indeed a significant fraction of the total star-formation in the Universe may occur in such events. However, there is also a population of mergers of two red galaxies, in which no star-formation occurs, an event usually referred to as a “dry merger” (Bell et al. 2006b; van Dokkum 2005).

A growing consensus of groups studying the high redshift Universe find that the luminous

red galaxies appear to grow in stellar mass over time (Bell et al. 2004; Willmer et al. 2005; Blanton 2006; Wake et al. 2006; Brown et al. 2007; Faber et al. 2007). This growth can occur in several ways. First, in principle they may have ongoing star-formation. This is very unlikely, since the red galaxies show little signs of such star-formation. Second, luminous blue galaxies may transform to red galaxies. This is also unlikely at the very luminous end, since the number density of luminous blue galaxies is far lower than that of red galaxies, even at high redshift. Third, and most likely, the luminous red galaxies may grow through either major or minor mergers.

If the change in the galaxy population over time is to be explained at least partly by mergers, we must be able to find these mergers before or as they occur in appropriate numbers. “Instantaneous” studies of the merger rate are complementary to, and must be consistent with, the global studies in the change of the galaxy population. To evaluate whether mergers can explain these changes, the work presented here is designed to measure the accretion or merger rate of companion galaxies into LRGs at redshift  $z \sim 0.25$ .

It is also the case that in the CDM paradigm for structure formation, galaxies reside in mass concentrations that are built from merging and accretion of smaller concentrations over cosmic time. It is unavoidable that this merging in the dark sector is associated, at some level, with merging of observable galaxies (e.g., Murali et al. 2002; Maller et al. 2006; Conroy et al. 2007).

There are many galaxy–galaxy merger rate estimates in the literature, which involve identifying a class of pre-merger close pairs (Carlberg et al. 1994; Patton et al. 1997; van Dokkum et al. 1999; Carlberg et al. 2000; Patton et al. 2000; Lin et al. 2004; Masjedi et al. 2006; Bell et al. 2006a; De Propris et al. 2007), a class of post-merger galaxies based on star-formation indicators (Quintero et al. 2004), or a class of currently merging sources based on disturbed or merging morphologies (Abraham et al. 1996; Conselice et al. 2003; van Dokkum 2005; Lotz et al. 2006; De Propris et al. 2007). In each case, the estimate of the merger rate proceeds by estimating the abundance of the class, some time interval over which they remain identifiably part of that class. The measurements of the LRG accretion rate presented here also follow this methodology. However, our measurements are more reliable than most previous measurements for a number of reasons. The first is that the LRGs form a very uniform, very massive population, as described above, and therefore dynamical times and dynamical-friction times relevant to close pairs are straightforward to estimate. The second is that we make maximal assumptions so as to put a strict *upper limit* on the accretion rate. This is interesting, because the upper limit we determine is on the low side of existing predictions and measurements. The third is that we use a technique for measuring the mean number of close pairs in real space, with no contamination by projected pairs, so our pre-merger

candidate list is clean of such interlopers (in a statistical sense).

Our technique for measuring the close pairs builds on previous work (Masjedi et al. 2006) in which we showed that we could measure projected correlation functions on extremely small scales (kpc to Mpc scales) without the need for complete spectroscopic samples. We used this method to overcome the fiber-collision incompleteness of the LRG sample in the SDSS. In addition, we showed that the clustering signal so measured can be deprojected and integrated to deduce close pair statistics and therefore a rate of merger events among the galaxies in the sample. We found that LRG–LRG mergers are extremely rare events and do not play a significant role in the growth of these galaxies, at least at low redshifts.

In this paper we expand this technique to measure not only the auto-correlation function of a set of galaxies, but the cross-correlation function of two different galaxy sets, only one of which requires spectroscopic information. We choose LRGs as our primary spectroscopic sample and we cross-correlate them with distinct subsamples of companion galaxies over a range of luminosities and colors. We convert these results into an accretion rate of luminosity—within each subsample—into LRGs. We can estimate a total accretion rate by this method with unprecedented precision.

Throughout this paper, all distances are comoving, calculated for a cosmological world model with  $(\Omega_m, \Omega_\Lambda) = (0.3, 0.7)$  and Hubble constant parameterized by  $H_0 \equiv 100 h \text{ km s}^{-1} \text{ Mpc}^{-1}$ . All magnitudes are AB.

## 2. Data

The SDSS (Stoughton et al. 2002; Abazajian et al. 2003; Abazajian et al. 2004) has performed an imaging and spectroscopic survey of  $\sim 10^4$  square degrees (Fukugita et al. 1996; Gunn et al. 1998; Gunn et al. 2006). Automated, real-time monitoring (Hogg et al. 2001), image processing (Lupton et al. 2001; Stoughton et al. 2002; Pier et al. 2003), photometric calibration (Smith et al. 2002; Ivezić et al. 2004; Tucker et al. 2006; Padmanabhan et al. 2007), galaxy target selection for spectroscopy (Strauss et al. 2002; Eisenstein et al. 2001), design of spectroscopic plates (Blanton et al. 2003a), and spectroscopic reductions have produced enormous, very uniform samples. Of the various SDSS subsamples, the one that uniformly maps the largest volume is the LRG sample (Eisenstein et al. 2001).

## 2.1. Spectroscopic subsample

The spectroscopic LRG sample is constructed from color-magnitude cuts in  $g$ ,  $r$ , and  $i$  bands to select galaxies that are likely to be luminous early-type galaxies at redshifts between 0.15 and 0.5. The selection is highly efficient and the redshift success rate is excellent. The sample is constructed to be close to volume-limited up to  $z = 0.36$ , with a dropoff in density toward  $z = 0.5$ . Because the LRG sample is so uniform, and because it occupies such a large volume, we have used it to demonstrate the homogeneity of the Universe (Hogg et al. 2005), to locate the baryon acoustic feature at low redshift (Eisenstein et al. 2005), and to measure clustering at intermediate and small scales (Zehavi et al. 2005; Masjedi et al. 2006).

This study uses a spectroscopic sample drawn from NYU LSS `sample14` (Blanton et al. 2005). This covers 3,836 square degrees and contains 55,000 LRGs with redshifts  $0.16 < z < 0.47$ . The subsample of LRGs used in this paper has luminosity and redshift ranges of  $-23.2 < [M_{0.3g} - 5 \log_{10} h] < -21.2$  mag and  $0.16 < z < 0.30$ . We restrict our sample to  $z < 0.30$  to allow measurement of cross-correlations between LRGs and much less luminous companions. The LRG absolute magnitudes include Galactic extinction corrections (Schlegel et al. 1998),  $K$  corrections (Blanton & Roweis 2007) and passive evolution corrections (the latter were applied only for the purposes of selecting a sample that does not substantially change with redshift). These cuts left 23043 LRGs in our spectroscopic subsample.

In the SDSS, spectroscopic targets were assigned to spectroscopic fiber plug plates with a tiling algorithm that ensures nearly complete samples (Blanton et al. 2003a). The angular completeness is characterized for each unique region of overlapping spectroscopic plates (“sector”) on the sky. An operational constraint of SDSS spectrographs, however, is that the physical size of the fiber coupling forces the angular separation of targets on any individual spectroscopic plate to be larger than 55 arcsec. This “fiber collision” constraint is partly reduced by having roughly 40 percent of the sky covered by overlapping plates, but it still results in  $\sim 7$  percent of targeted galaxies not having measured redshifts. Because this project involves cross-correlating spectroscopic and imaging objects, this fiber collision limit only comes into our analysis in our weighting scheme to account for incompleteness; it does not affect our pair counts directly.

For each galaxy  $j$  in the spectroscopic subsample we compute a weight  $p_j$  that accounts statistically for the spectroscopic incompleteness coming from fiber collisions. We calculate this weight by running a two-dimensional friends-of-friends grouping algorithm on the SDSS target parent sample in `sample14`, with a 55 arcsec linking length. This procedure emulates the SDSS tiling algorithm (Blanton et al. 2003a). Within each “collision group” made by the friends-of-friends algorithm, we find the number of objects with measured spectroscopic

redshifts and divide by the total number. The inverse of this ratio is a weight  $p_j$  assigned to each spectroscopic LRG to account for survey incompleteness.

We have created large catalogs of randomly distributed points based on the SDSS subsample angular and radial (redshift distribution) models. These catalogs match the redshift distribution of the LRGs and are isotropic within the survey region. These catalogs allow us to check the survey completeness of any given volume and provide a homogeneous baseline (expected numbers) for the tests that follow.

For each random point  $j$  we compute a weight  $f_j$  that accounts for the incompleteness of the spectroscopic survey in that point’s region of the sky *not* due to fiber collision but due to all the other selection effects in the survey. The `sample14` package provides the angular geometry of the spectroscopic survey expressed in terms of spherical polygons. The geometry is complicated: the spectroscopic plates are circular and overlap, while the imaging is in long strips on the sky, and there are overlap regions for some plates that have not yet been observed. The resulting spherical polygons track all these effects and characterize the geometry in terms of “sectors”, each being a unique region of overlapping spectroscopic plates. In each sector, we count the number of possible targets (LRG, Main, and Quasar), excluding those missed because of fiber collisions, and the number of these whose redshifts were determined. We weight the points in the random catalog matched to the spectroscopic LRGs by the inverse of the ratio of these numbers ( $f_j$ ). In truth, the priority of all targets are not equal, such that LRGs always “lose” to quasar candidates, but the LRG priority is equal to that of the dominant MAIN targets. Only about 12 percent of the fibers are assigned to quasars, hence quasar-LRG collisions are rare and this priority bias is small.

We are required to treat the fiber collision incompleteness  $p_j$  and overall incompleteness  $f_j$  factors separately, because the former is strongly correlated with LRG environment, and there can be physical differences between LRGs in high and low density environments.

## 2.2. Imaging subsamples

For our imaging data we use the full imaging sample of the SDSS imaging catalog in the DR4plus footprint, which completely covers `sample14` and is equivalent to the SDSS Data Release 5. After correcting for Galactic extinction, we applied an  $i$ -band apparent magnitude cut of  $m_i < 21$  mag. This cut guarantees completeness in the redshift range  $z < 0.30$ ,  $K$ -corrected absolute magnitude range  $[M_{0.3i} - 5 \log_{10} h] < -18$  mag. The  $^{0.3}g$ ,  $^{0.3}r$ , and  $^{0.3}i$  bandpasses are the SDSS  $g$ ,  $r$ , and  $i$  bandpasses shifted blueward by a factor of 1.3 so that  $K$  corrections for galaxies at  $z = 0.3$  become trivial (e.g., Hogg et al. 2002a; Blanton et al.

2003b). We applied an additional surface-brightness cut of  $\mu < 28$  mag in  $1 \text{ arcsec}^2$  in  $g$ ,  $r$  and  $i$ . The surface-brightness cut is far below the SDSS detection limit; it cleans the data of the obvious mis-measurements of the Petrosian aperture and other extended-source data artifacts.

We cannot  $K$ -correct individual galaxies in the imaging subsample once and for all, because we do not have spectroscopic redshifts for them, but each time we consider a *pair* of galaxies, one from the spectroscopic subsample and one from the imaging subsample, we fictitiously assign the spectroscopic redshift to the imaging galaxy. This allows us to calculate for each imaging galaxy in each spectroscopic–imaging pair a “temporary”  $K$ -corrected  $^{0.3}i$ -band absolute magnitude and  $[^{0.3}g - ^{0.3}r]$  color for the purposes of that pair. We discard these values and compute new ones when the imaging galaxy is used in another pair with another spectroscopic galaxy.

We calculated the  $K$ -corrections using the code `kcorrect` (Blanton & Roweis 2007). This code is accurate but too slow to calculate the  $K$ -corrections individually for the number of pairs ( $\sim 10^9$ ) found in the cross-correlations. To save time, we computed the  $K$ -correction on a grid of colors in advance. We took galaxies from the SDSS Main Sample as representative of all galaxy types. We computed their  $K$ -corrections on a grid of redshifts between 0.16 and 0.30 (the redshift limits of our spectroscopic subsample). We saved the mean  $K$ -correction in a grid of observed  $[g - r]$  color,  $[r - i]$  color, and redshift. Thereafter we interpolated this cube when calculating the  $K$ -correction for an galaxy in any imaging subsample. This speeds up the  $K$ -correction procedure immensely and only introduces percent-level errors in the results.

We have created large catalogs of randomly distributed points, with the angular distribution of the imaging data subsamples.

### 3. Method and results

As we describe in this section, we cross-correlate galaxies in a spectroscopic subsample  $s$  (of LRGs in this case) with galaxies in an imaging subsample  $i$  to obtain the real-space, projected cross-correlation function  $w_{si}(r_p)$  as a function of tangential projected separation  $r_p$ . We de-project this projected cross-correlation function to obtain the true, three-dimensional, real-space cross-correlation function  $\xi_{si}(r)$  as a function of real-space separation  $r$ . We use this three-dimensional cross-correlation function and dynamical arguments to place limits on the accretion rate of objects from subsample  $i$  into objects from subsample  $s$ , and therefore the mass growth rate of LRGs.

### 3.1. Projected cross-correlation function

In analogy to the definition of auto-correlation function, the three-dimensional real-space cross-correlation function  $\xi_{si}(r)$  of two subsamples of galaxies  $s$  and  $i$ , is defined as the excess probability of finding a galaxy from subsample  $s$  at a distance  $r$  from a galaxy from the subsample  $i$ , relative to the “null” Poisson prediction. If we take two small comoving volumes  $dV_s$  and  $dV_i$ , in which we look for galaxies from subsamples  $s$  and  $i$  respectively, separated by a distance  $r$ , the expected number of pairs  $dN_{si}$  with one galaxy coming from subsample  $s$  and the other from subsample  $i$  is:

$$dN_{si} = n_s n_i [1 + \xi_{si}(r)] dV_s dV_i \quad , \quad (1)$$

where  $n_s$  and  $n_i$  are the three-dimensional comoving number densities of subsamples  $s$  and  $i$  respectively.

The projected two-dimensional cross-correlation function  $w_{si}(r_p)$  is related to the three-dimensional real-space correlation function  $\xi_{si}(r)$  by a projection over the component  $\pi$  of the separation along the line of sight

$$w_{si}(r_p) = \int d\pi \xi_{si} \left( \sqrt{r_p^2 + \pi^2} \right) \quad . \quad (2)$$

The two-dimensional function  $w_{si}(r_p)$  has dimensions of length. Because in practice the correlation function  $\xi_{si}(r)$  is very large at small scales, the integral is dominated by scales  $\pi < r_p$ . Observationally,  $w_{si}(r_p)$  is much more accessible than  $\xi_{si}(r)$ , because the radial component of the separation is never well measured (and not measured at all in the work presented here).

Following the approach we have used previously (Masjedi et al. 2006), we measure  $w_{si}(r_p)$  schematically as a difference of two ratios:

$$n_i w_{si}(r_p) = \frac{D_s D_i}{D_s R_i} - \frac{R_s D_i}{R_s R_i} \quad , \quad (3)$$

where  $n_i$  is the average comoving three-dimensional volume density of the imaging subsample, the symbols  $D_s$  and  $D_i$  represent the spectroscopic and imaging data subsamples, and  $R_s$  and  $R_i$  represent the random catalogs matched to the spectroscopic and imaging subsamples respectively. The product of a volume density and a length,  $n_i w_{si}(r_p)$  has dimensions of inverse (comoving) area. In a rough sense, the first term on the right-hand side of equation (3) measures the abundance of pairs, and the second term subtracts the mean background level. The procedure described here has been tested with simulations and shown to deliver an unbiased measure of the correlation function (Masjedi et al. 2006).



The main difference between equation (3) and our previous work (Masjedi et al. 2006) is that the number density  $n_i$  that enters on the left-hand side is the number density of the imaging subsample, which we cannot determine explicitly within this data set since, by construction, the imaging subsample has no (or few) spectroscopic redshifts. We can only measure robustly the product  $n_i w_{si}(r_p)$ . Fortunately, for the purposes of estimating the merger rate, we need only this product, and not either quantity separately.

The right-hand side of Equation (3) includes a spectroscopic–imaging pair-count factor  $D_s D_i$ :

$$D_s D_i = \frac{\sum_{j \in \mathbb{D}_s \mathbb{D}_i} p_j}{\sum_{k \in \mathbb{D}_s} p_k} \quad , \quad (4)$$

where the top sum is over pairs  $j$  with one member taken from the spectroscopic subsample and one from the imaging subsample in some bin of transverse radii  $r_p$ , the bottom sum is over galaxies  $k$  from the spectroscopic subsample, and  $p_j$  is the weight given to the spectroscopic galaxy in pair  $j$  that accounts for fiber-collision incompleteness as described above. Being a sum of dimensionless weights, this factor  $D_s D_i$  is dimensionless.

There is a spectroscopic–random pair-count factor  $D_s R_i$ :

$$D_s R_i = \frac{\sum_{j \in \mathbb{D}_s \mathbb{R}_i} p_j}{\sum_{k \in \mathbb{D}_s} p_k \left[ \frac{d\Omega}{dA} \right]_k \frac{dN}{d\Omega}} \quad , \quad (5)$$

where the top sum is over pairs  $j$  with one member taken from the spectroscopic subsample and one taken from the random catalog matched to the imaging subsample, the bottom sum is over galaxies  $k$  in the spectroscopic subsample,  $\left[ \frac{d\Omega}{dA} \right]_k$  is the inverse square of the comoving distance to the spectroscopic galaxy  $k$ , and  $\frac{dN}{d\Omega}$  is the number density of the random imaging catalog per solid angle. The product of these two derivatives gives the average number of random imaging objects per unit comoving area around each spectroscopic galaxy, so this factor  $D_s R_i$  has dimensions of comoving area.

There is a random–imaging pair-count factor  $R_s D_i$ :

$$R_s D_i = \frac{\sum_{j \in \mathbb{R}_s \mathbb{D}_i} f_j}{\sum_{k \in \mathbb{R}_s} f_k} \quad , \quad (6)$$

where the top sum is over pairs  $j$  with one member taken from the random catalog matched to the spectroscopic subsample and one taken from the imaging subsample, the bottom sum is over points in the random catalog matched to the spectroscopic subsample, and  $f_j$  is the weight given to the random point in pair  $j$  that accounts for the incompleteness of the spectroscopic survey in that point’s region of the sky *not* due to fiber collisions, as described above. This factor  $R_s D_i$  is dimensionless.

There is a random–random pair-count term  $R_s R_i$ :

$$R_s R_i = \frac{\sum_{j \in \mathbb{R}_s \mathbb{R}_i} f_j}{\sum_{k \in \mathbb{R}_s} f_k \left[ \frac{d\Omega}{dA} \right]_k \frac{dN}{d\Omega}} \quad , \quad (7)$$

similar to the above but for pairs  $j$  with one member taken from the random catalog matched to the spectroscopic subsample and one taken from the random catalog matched to the imaging subsample. This factor  $R_s R_i$  has dimensions of comoving area.

In measuring the four factors on the right-hand side of Equation (3), we have used 2 imaging-galaxy color bins separating the blue and red imaging galaxies in  $[^{0.3}g - ^{0.3}r]$  color, 20 imaging-galaxy luminosity bins, which we choose to cover the range  $-24 < [M_{0.3i} - 5 \log_{10} h] < -18$  mag but have roughly the same number of imaging galaxies in each, and 15 bins in projected transverse separation  $r_p$  between the LRG and the accompanying galaxy, covering the range of  $0.01 < r_p < 8 h^{-1}$  Mpc with logarithmic spacing.

In practice, to compute the factors, we bin all the spectroscopic–imaging pairs according to the imaging galaxy color, the imaging galaxy luminosity, and the comoving projected separation  $r_p$  of the pair. As described above, the  $K$  corrections and separations are computed for each pair using the redshift of the spectroscopic galaxy. We perform the sums given in Equations (4) through (7) in each bin separately and thereby construct the  $w_{si}$  estimator given in Equation (3).

Figures 1 and 2 show the measurements of  $n_i w_{si}(r_p)$  for red and blue companion galaxies respectively. We have combined the 20 luminosity bins into 5 to simplify the figures. The error bars are estimated using jackknife resampling covariance matrix with 100 subsamples made contiguous and compact on the sky (based on SDSS “targetting chunks”) to be as conservative as possible with regards to correlated calibration and selection errors. Note that the error bars for each subsample are smallest on kpc scales and become larger for both the smaller and larger scales. On smaller scales this is due to shot noise; the smaller the separations the fewer the pair counts. On scales larger than a few  $h^{-1}$  kpc, the errors grow both due to cosmic variance and the fact that our method becomes more and more vulnerable to

interlopers on larger scales where the clustering power is weaker and background subtraction is more noisy. These effects generate high correlations among the errors of different bins, and explains the smoothness of the curves in Figures 1 and 2 despite the large uncertainties in each bin.

### 3.2. Three-dimensional statistics

Under the assumption of spherical symmetry, the two-dimensional, projected cross-correlation function  $w_{si}(r_p)$  can be “deprojected” into the three-dimensional, real-space correlation function  $\xi_{si}(r)$ :

$$n_i \xi_{si}(r) = -\frac{1}{\pi} \int_r^\infty \frac{dr_p}{\sqrt{r_p^2 - r^2}} \frac{d[n_i w_{si}(r_p)]}{dr_p} \quad , \quad (8)$$

where we have kept this deprojection in terms of the measurable product  $n_i w_{si}(r_p)$ .

The correlation function can be converted to pair counts; similarly the cross-correlation function can be converted into the mean number  $N_i$  of galaxies from a specific imaging subsample  $i$  within a given small three-dimensional separation  $r_{\text{close}}$  of a member of the spectroscopic subsample  $s$ :

$$N_i = 4 \pi n_i \int_0^{r_{\text{close}}} r^2 dr [1 + \xi_{si}(r)] \approx 4 \pi \int_0^{r_{\text{close}}} r^2 dr [n_i \xi_{si}(r)] \quad , \quad (9)$$

where we have used the fact that at small scales  $\xi_{si} \gg 1$  and the term in brackets in the approximate expression is the quantity we can de-project from the two-dimensional projected cross-correlation function  $n_i w_{si}(r_p)$ . So we can measure the close pair fraction for every subsample for which we can measure the cross-correlation function.

### 3.3. Merger rate

Conversion of a pair fraction measurement into a merger rate requires a time-scale  $t_{\text{merge},i}$  over which the mean galaxy from imaging subsample  $i$  within separation  $r_{\text{close}}$  will merge with the mean LRG from subsample  $s$ . The merger rate estimate  $\Gamma_i$  of galaxies from sample  $i$  into galaxies from sample  $s$  per galaxy (from  $s$ ) per unit time is

$$\Gamma_i = \frac{N_i}{t_{\text{merge},i}} \quad , \quad (10)$$

and the mean fractional rate of growth of luminosity of a galaxies from subsample  $s$  from accretion of galaxies from subsample  $i$  is

$$\frac{1}{\langle L_s \rangle} \left[ \frac{dL_s}{dt} \right]_i = \frac{N_i \langle L_i \rangle}{t_{\text{merge},i} \langle L_s \rangle} \quad , \quad (11)$$

where  $\langle L_s \rangle$  is the mean luminosity of galaxies from subsample  $s$  and  $\langle L_i \rangle$  is the mean luminosity of galaxies from subsample  $i$ .

The shortest conceivable merger time  $t_{\text{merge},i}$  estimate (which produces the largest conceivable estimate of the merger rate) is the orbital time  $t_{\text{orbit}}$ . A more realistic estimate is a time  $t_{\text{dyn},i}$  based on dynamical friction. But in principal all of these times can be underestimates (and hence any merger rate based on close pairs can be an overestimate) because there is undoubtedly a large number of close pairs that will not merge on any short timescale. In what follows, we present the orbital time  $t_{\text{orbit}}$  and dynamical friction time  $t_{\text{dyn},i}$  as two options, but then interpret our merger rate estimates as upper limits.

All of these merger rate estimates depend, in principle, on the radius  $r_{\text{close}}$  inside of which we have counted close companions. However, over the range of interest in Figures 1 and 2,  $w_{si}(r_p)$  scales (something) like  $r_p$ ,  $\xi_{si}(r)$  scales (something) like  $r^2$  and  $N_i$  scales (something) like  $r_{\text{close}}$ . Similarly, both time-scales (orbital and dynamical-friction) scale like  $r_{\text{close}}$ . For this reason, the inferred merger and accretion rates (which are based on ratios of  $N_i$  with the timescales) do *not* depend strongly on the choice of  $r_{\text{close}}$ .

The average orbital velocity for a companion around a more massive galaxy with velocity dispersion  $\sigma_v$  is roughly 1.5 times the velocity dispersion, so

$$t_{\text{orbit}} \approx \frac{2 \pi r_{\text{close}}}{1.5 \sigma_v} \quad . \quad (12)$$

This is the shortest conceivable mean merger time (we have included the factor of 1.5 to be conservative). The fractional luminosity accretion rate estimate for this assumed time-scale is shown with dashed lines in Figure 3 as a function of the luminosity of imaging subsample  $i$  for red and blue imaging galaxies. The per-subsample merger rates have been divided by the absolute-magnitude bin width so that the total fractional accretion rate is the area under (integral of) the curves.

The Chandrasekhar approximation to dynamical friction is longer than the dynamical time by a factor roughly equal to the ratio of the mass of the heavier galaxy to the lighter one. This approximation may actually be an underestimate of the total merger time found in explicit  $N$ -body simulations (Boylan-Kolchin et al. 2007), which serves to strengthen the interpretation of our merger rate estimate as an upper limit. For our case, the approximation

becomes

$$t_{\text{dyn},i} = t_{\text{orbit}} \frac{\langle m_s \rangle}{\langle m_i \rangle} \quad , \quad (13)$$

where  $\langle m_s \rangle$  and  $\langle m_i \rangle$  are the averages of the masses of the spectroscopic and imaging subsamples respectively, and we have assumed  $\langle m_s \rangle > \langle m_i \rangle$ . Keeping things observational, we do not try to measure masses for galaxies in this work. Instead, we make the naive assumption that a galaxy’s mass is directly proportional to its  $^{0.3}i$ -band luminosity and therefore we use the ratio of the luminosities instead of the masses. The  $^{0.3}i$ -band luminosity is very close to the rest frame  $r$ -band luminosity. This assumption works fairly well for the mass ratios of red imaging galaxies to the spectroscopic galaxies (which are LRGs) but tends to over estimate the masses of the blue companions. This bias leads to an underestimation of merger time-scales and hence an overestimation of the fractional accretion rate for blue companions.

The solid lines in Figure 3 show the calculated fractional luminosity growth of the LRGs assuming the dynamical friction time-scale  $t_{\text{dyn},i}$  for the mergers. The per-subsample merger rates have been divided by the absolute-magnitude bin width so that the total fractional accretion rate is the area under (integral of) the curves. If the results in Figure 3 are naively interpreted as fractional *mass* accretion rates (they are fractional luminosity rates), the blue galaxies are doubly overestimated, because both the merger rate (inverse timescale) and the delivered mass have been over-estimated.

Under the orbital time-scale assumption, the growth curve in Figure 3 peaks near the magnitude of  $L^*$  galaxies. This represents fact that most of the light in the Universe, even near LRGs, is in  $L^*$  galaxies. Under the dynamical friction assumption, the curves shift to more luminous, more massive, galaxies; lighter galaxies linger around the LRG for a longer time.

The maximal fractional luminosity accretion rate (the sum of the integrals under the dashed curves in Figure 3) is  $[5.6 \pm 0.2]$  percent  $\text{Gyr}^{-1}$ , but this rate is unrealistically high; certainly pairs with large mass differences do not merge in an orbital time! The dynamical-friction rate is  $[1.7 \pm 0.1]$  percent  $\text{Gyr}^{-1}$ , and is also probably an overestimate because at least some physical pairs are not on the path to rapid merging.

Table 1 gives the derived fractional luminosity growth from every imaging subsample for both the orbital time-scale assumption and the dynamical friction time-scale assumption as a function of the luminosity and color of the subsamples.

#### 4. Discussion

We have combined Sloan Digital Sky Survey (SDSS) spectroscopic data on 23043 luminous red galaxies (LRGs) with SDSS imaging data on enormous subsamples of fainter galaxies to measure cross-correlations. We have measured the projected two-dimensional cross-correlation functions  $w_{si}(r_p)$  on very small scales ( $0.01 < r_p < 8 h^{-1}$  Mpc) between spectroscopic LRGs (“s”) with luminosities  $[M_{0.3i} - 5 \log_{10} h] \approx -22.75$  mag and many subsamples of imaging galaxies (“i”) with luminosities  $[M_{0.3i} - 5 \log_{10} h] < -18$  mag. The imaging limit is 50 times or 4.25 mag fainter than the mean LRG; the samples of companion galaxies cover a broad range in color and magnitude. In addition, the large volume of the SDSS LRG sample allows us to cut the companion galaxies into many distinct subsamples with different luminosities and colors but nonetheless measure the clustering as a function of these properties with high signal-to-noise. The principal limitation arises from the lack of spectroscopic information on the companion galaxies; this makes it impossible to precisely measure the real-space number densities for the companion subsamples. We cannot disentangle the clustering power from the number density; we only measure the product  $n_i w_{si}(r_p)$  but not either  $n_i$  or  $w_{si}(r_p)$  separately.

Figures 1 and 2 show the results of these measurements of  $n_i w_{si}(r_p)$  for red and blue galaxies respectively. In both figures several characteristic transition scales are visible. The sharp break at  $r_p \approx 2 h^{-1}$  Mpc and the less-sharp transition at  $r_p \approx 0.3 h^{-1}$  Mpc in the curves can be explained in the context of the “halo occupation” picture of galaxy clustering (Peacock & Smith 2000; Scoccimarro et al. 2001; Berlind & Weinberg 2002). If galaxies are residing within dark matter halos then the clustering of the galaxies on scales larger than halos is determined by the clustering of the dark matter halos that host them, plus statistics of the occupation of halos by galaxies. In this picture, the first transition at  $r_p \approx 2 h^{-1}$  Mpc locates the size of the largest halos that host LRGs—the largest halos in the Universe. At larger separations, at  $r_p > 2 h^{-1}$  Mpc, this is the regime in which all LRG–galaxy pairs come from two separate halos (the “two-halo” regime). Inside this scale, at  $0.3 < r_p < 2 h^{-1}$  Mpc, the galaxy–LRG pairs are a mix of pairs, in some of which the companion galaxy belongs to the same halo as the LRG and in some of which the galaxy belongs to a separate halo. This “mixed” regime comes from the fact that LRGs reside in a range of halo sizes. The inner limit of this regime is at  $r_p \approx 0.3 h^{-1}$  Mpc, depending on the luminosity of the imaging galaxy subsample  $i$  in question. This inner scale is close to the virial size of the smallest halo that can host an LRG (plus the virial size of the smallest halo that can host a companion galaxy from the imaging subsample  $i$ ). At smaller scales, at  $r_p < 0.3 h^{-1}$  Mpc, all the galaxies belong to the same halo as the LRG halo (the “one-halo” regime). Here the clustering represents the mean radial profile of the halos mixed with details of galaxy evolution. Figure 1 shows an increase in the clustering of blue galaxies at  $r_p \approx 50 h^{-1}$  kpc toward the central regions of

the halo. This could be caused by a boost of star formation in these galaxies, which makes them more luminous and places them in higher luminosity bins in our calculation.

Finally, both Figures show a sharp drop in the clustering power on scales  $r_p < 30 h^{-1}$  kpc. This could be due to failure of the object detection software of the SDSS (e.g., Masjedi et al. 2006), or it could be a real effect from disintegration of galaxies by dynamical friction or other tidal stripping expected in some galaxy evolution models.

We integrate the de-projected, three-dimensional cross-correlation functions  $n_i \xi_{si}(r)$  for each imaging subsample  $i$  on very small scales to calculate the average number of galaxies that are in dynamical pairs with each LRG. We use two different time-scales for merger events to calculate merger rates. The first is the orbital time  $t_{\text{orbit}}$ , equivalent to assuming that all galaxies merge in one orbit. This is the shortest time imaginable to merge, so it provides a strict upper limit on the merger rate. The second time-scale is the dynamical friction time-scale  $t_{\text{dyn},i}$  for which we approximate the merger time with a linear function of the mass ratio  $\langle m_s \rangle / \langle m_i \rangle$  of the mean galaxies from the two samples. This is equivalent to assuming that equal-mass (LRG–LRG) mergers take the one-orbit time, but pairs of galaxies with more different masses take longer times to merge.

We use the two time-scales to calculate both a strict upper limit to the merger rate and a more realistic rate, although even the dynamical friction time-scale calculation involves assuming that essentially all close pairs merge. For both time-scales we have measured the fraction of LRG luminosity that is added to the LRG through mergers of galaxies from each imaging subsample  $i$  per Gyr. The fractional luminosity growth for LRGs through mergers as a function of the color and magnitude of the merging companions is shown in Figure 3.

Most of the luminosity brought into LRGs by merging is brought by red companions or “dry mergers,” and most of it is brought by galaxies near (or above)  $L^*$ . The contribution to growth decreases with decreasing luminosity at the faint end; the curves essentially to zero by  $[M_{0.3i} - 5 \log_{10} h] = -18$  mag. Calculation of the total amount of luminosity brought in by merger activities does not require consideration of fainter companion galaxies.

Integration of Figure 3 over companion absolute magnitude yields the total fractional amount of LRG luminosity growth from mergers. Under the maximal one-orbit merger time assumption, we find that the total fractional growth rate is strictly smaller than  $[5.6 \pm 0.2]$  percent  $\text{Gyr}^{-1}$ . Under the more realistic dynamical friction assumption, we find that the total fractional growth rate is  $[1.7 \pm 0.1]$  percent  $\text{Gyr}^{-1}$  where only about one-tenth of that is through “wet mergers” (blue companions) and the rest is through dry mergers (red companions).

Our results are *not* consistent, at face value, with most morphological measurements of

the merger rate—measures that involve identification of merging galaxies by their appearances—most of which find rates on the order of ten percent per Gyr or of order unity over a Hubble time (e.g., Abraham et al. 1996; Conselice et al. 2003; van Dokkum 2005; Lotz et al. 2006; though see also De Propris et al. 2007). Our method for inferring the merger rate suffers—as all these other investigators’ methods do—from uncertainties in merger timescales. However, we avoid all issues related to morphological selection of merging systems or merger remnants, which tend to introduce subjectivity, and we avoid uncertainties related to line-of-sight projections because we work with the true three-space correlation function. Our method is therefore much more precise than other methods. Furthermore, because merging cannot happen on timescales shorter than a dynamical time, our upper limit is extremely robust (and not made uncertain by projection effects).

Our merger rate estimate can be reconciled with other estimates if we assume that either (1) the merger rate is an extremely strong function of the primary galaxy mass (since we only investigate the rate for the most massive galaxies in the Universe), or (2) merging produces observable distortions to galaxy morphologies (e.g., tidal tails) that last for many dynamical times, or (3) significant morphological signs of merging can be raised by very frequent, very minor mergers, which don’t contribute much to the build-up of mass. Our results are more consistent with measures of the merger rate based on counts of close pairs (Carlberg et al. 1994; Patton et al. 1997; van Dokkum et al. 1999; Carlberg et al. 2000; Patton et al. 2000; Lin et al. 2004; Masjedi et al. 2006; Bell et al. 2006a), but even there, our results are on the low side.

Our results are also lower than any accretion or merger predicted in theories of galaxy formation in a cosmological context (Murali et al. 2002; Maller et al. 2006; Conroy et al. 2007), but we caution that no predictions have been made for exactly what we have observed, and that galaxy–galaxy merging occurs at length and dynamical scales where cosmological simulations are not completely reliable.

There are three respects in which the luminosity growth shown in the solid lines in Figure 3—the more “realistic” estimates—are nonetheless over-estimates or upper limits on the true fractional mass growth for LRGs. First, we are assuming that the vast majority of pairs do merge as quickly as dynamical friction allows. This is not true for close pairs in high velocity-dispersion environments. In addition, even when the pairs are bound the Chandrasekhar formula may be an overestimate (Boylan-Kolchin et al. 2007). Second, the blue galaxies have both their masses over-estimated and their dynamical friction times under-estimated with a constant mass-to-light ratio assumption, so the blue galaxies do not contribute as much mass as Figure 3 implies. Third, we are assuming that all the stars in the companion galaxies will end up in the central LRGs. Recent work has suggested that



this is not the case and in fact up to 50 percent of the stars in the companions could be stripped off the companion before the merger is complete and contribute to the intra-cluster light instead of the luminosity of the LRG (Lin et al. 2004). This suggests that even our dynamical friction assumption could still be an upper limit on the growth of the LRGs.

These results are consistent with recent results on the evolution of the luminosity function of the red galaxies since redshift  $z \sim 1$ , which find modest evolution (Bell et al. 2004; Blanton 2006; Wake et al. 2006; Faber et al. 2007; Brown et al. 2007). If we take our results at face value and assume that the growth happens at a non-evolving rate, we expect the LRGs to grow by about  $\approx 10$  percent between redshift  $z = 1$  and  $z = 0.1$  (a period of  $\approx 6$  Gyr).

It is a pleasure to thank Eric Bell, Andreas Berlind, Daniel Eisenstein, and Ari Maller for valuable input. Some of this research was performed while DWH was generously hosted by Hans-Walter Rix and the Max-Planck-Institut für Astronomie. This research was partially supported by the National Aeronautics and Space Administration (NASA; grant NAG5-11669) and the National Science Foundation (NSF; grant AST-0428465). This research made use of the NASA Astrophysics Data System. It also made use of the “idlutils” codebase maintained by David Schlegel, Wayne Landsman, Doug Finkbeiner, and others.

This research made use of public SDSS data. Funding for the SDSS and SDSS-II has been provided by the Alfred P. Sloan Foundation, the Participating Institutions, the National Science Foundation, the U.S. Department of Energy, the National Aeronautics and Space Administration, the Japanese Monbukagakusho, the Max Planck Society, and the Higher Education Funding Council for England. The SDSS Web Site is <http://www.sdss.org/>.

The SDSS is managed by the Astrophysical Research Consortium for the Participating Institutions. The Participating Institutions are the American Museum of Natural History, Astrophysical Institute Potsdam, University of Basel, University of Cambridge, Case Western Reserve University, University of Chicago, Drexel University, Fermilab, the Institute for Advanced Study, the Japan Participation Group, Johns Hopkins University, the Joint Institute for Nuclear Astrophysics, the Kavli Institute for Particle Astrophysics and Cosmology, the Korean Scientist Group, the Chinese Academy of Sciences, Los Alamos National Laboratory, the Max-Planck-Institute for Astronomy, the Max-Planck-Institute for Astrophysics, New Mexico State University, Ohio State University, University of Pittsburgh, University of Portsmouth, Princeton University, the United States Naval Observatory, and the University of Washington.

## REFERENCES

- Abazajian, K. et al. 2003, *AJ*, 126, 2081
- Abazajian, K. et al. 2004, *AJ*, 128, 502
- Abraham, R. G., Tanvir, N. R., Santiago, B. X., Ellis, R. S., Glazebrook, K., & van den Bergh, S. 1996, *MNRAS*, 279, L47
- Baldry, I. K., Glazebrook, K., Brinkmann, J., Ivezić, Ž., Lupton, R. H., Nichol, R. C., & Szalay, A. S. 2004, *ApJ*, 600, 681
- Balogh, M. L., Baldry, I. K., Nichol, R., Miller, C., Bower, R., & Glazebrook, K. 2004, *ApJ*, 615, L101
- Barnes, J. E. & Hernquist, L. 1996, *ApJ*, 471, 115
- Barton, E. J., Geller, M. J., & Kenyon, S. J. 2000, *ApJ*, 530, 660
- Bell, E. F., Phleps, S., Somerville, R. S., Wolf, C., Borch, A., & Meisenheimer, K. 2006a, *ArXiv Astrophysics e-prints*
- Bell, E. F., Wolf, C., Meisenheimer, K., Rix, H.-W., Borch, A., Dye, S., Kleinheinrich, M., Wisotzki, L., & McIntosh, D. H. 2004, *ApJ*, 608, 752
- Bell, E. F. et al. 2006b, *ApJ*, 640, 241
- Berlind, A. A. & Weinberg, D. H. 2002, *ApJ*, 575, 587
- Blanton, M. R. 2006, *ApJ*, 648, 268
- Blanton, M. R., Lin, H., Lupton, R. H., Maley, F. M., Young, N., Zehavi, I., & Loveday, J. 2003a, *AJ*, 125, 2276
- Blanton, M. R. & Roweis, S. 2007, *AJ*, 133, 734
- Blanton, M. R. et al. 2003b, *ApJ*, 594, 186
- Blanton, M. R. et al. 2005, *AJ*, 129, 2562
- Boylan-Kolchin, M., Ma, C.-P., & Quataert, E. 2007, *ArXiv e-prints*, 707
- Brown, M. J. I., Dey, A., Jannuzi, B. T., Brand, K., Benson, A. J., Brodwin, M., Croton, D. J., & Eisenhardt, P. R. 2007, *ApJ*, 654, 858

- Carlberg, R. G., Pritchett, C. J., & Infante, L. 1994, *ApJ*, 435, 540
- Carlberg, R. G. et al. 2000, *ApJ*, 532, L1
- Conroy, C., Ho, S., & White, M. 2007, *MNRAS*, 379, 1491
- Conselice, C. J., Bershadsky, M. A., Dickinson, M., & Papovich, C. 2003, *AJ*, 126, 1183
- Cox, T. J., Dutta, S. N., Di Matteo, T., Hernquist, L., Hopkins, P. F., Robertson, B., & Springel, V. 2006, *ApJ*, 650, 791
- De Propris, R., Conselice, C. J., Driver, S. P., Liske, J., Patton, D., Graham, A., & Allen, P. 2007, *ArXiv e-prints*, 0705.2528
- Eisenstein, D. J., Blanton, M., Zehavi, I., Bahcall, N., Brinkmann, J., Loveday, J., Meiksin, A., & Schneider, D. 2005, *ApJ*, 619, 178
- Eisenstein, D. J. et al. 2001, *AJ*, 122, 2267
- Eisenstein, D. J. et al. 2005, *ApJ*, 633, 560
- Faber, S. M. et al. 2007, *ApJ*, 665, 265
- Fukugita, M., Ichikawa, T., Gunn, J. E., Doi, M., Shimasaku, K., & Schneider, D. P. 1996, *AJ*, 111, 1748
- Gunn, J. E., Carr, M. A., Rockosi, C. M., Sekiguchi, M., et al. 1998, *AJ*, 116, 3040
- Gunn, J. E. et al. 2006, *AJ*, 131, 2332
- Hogg, D. W., Baldry, I. K., Blanton, M. R., & Eisenstein, D. J. 2002a, *astro-ph/0210394*
- Hogg, D. W., Eisenstein, D. J., Blanton, M. R., Bahcall, N. A., Brinkmann, J., Gunn, J. E., & Schneider, D. P. 2005, *ApJ*, 624, 54
- Hogg, D. W., Finkbeiner, D. P., Schlegel, D. J., & Gunn, J. E. 2001, *AJ*, 122, 2129
- Hogg, D. W. et al. 2002b, *AJ*, 124, 646
- Ivezić, Ž. et al. 2004, *Astronomische Nachrichten*, 325, 583
- Lambas, D. G., Tissera, P. B., Alonso, M. S., & Coldwell, G. 2003, *MNRAS*, 346, 1189
- Lin, L. et al. 2004, *ApJ*, 617, L9
- Lotz, J. M., Madau, P., Giavalisco, M., Primack, J., & Ferguson, H. C. 2006, *ApJ*, 636, 592

- Lupton, R. H., Gunn, J. E., Ivezić, Z., Knapp, G. R., Kent, S., & Yasuda, N. 2001, in ASP Conf. Ser. 238: Astronomical Data Analysis Software and Systems X, Vol. 10, 269
- Maller, A. H., Katz, N., Kereš, D., Davé, R., & Weinberg, D. H. 2006, *ApJ*, 647, 763
- Masjedi, M. et al. 2006, *ApJ*, 644, 54
- Murali, C., Katz, N., Hernquist, L., Weinberg, D. H., & Davé, R. 2002, *ApJ*, 571, 1
- Naab, T. & Burkert, A. 2003, *ApJ*, 597, 893
- Negroponte, J. & White, S. D. M. 1983, *MNRAS*, 205, 1009
- Nikolic, B., Cullen, H., & Alexander, P. 2004, *MNRAS*, 355, 874
- Padmanabhan, N. et al. 2007, *ArXiv*, astro-ph/0703454
- Patton, D. R., Carlberg, R. G., Marzke, R. O., Pritchett, C. J., da Costa, L. N., & Pellegrini, P. S. 2000, *ApJ*, 536, 153
- Patton, D. R., Pritchett, C. J., Yee, H. K. C., Ellingson, E., & Carlberg, R. G. 1997, *ApJ*, 475, 29
- Peacock, J. A. & Smith, R. E. 2000, *MNRAS*, 318, 1144
- Pier, J. R., Munn, J. A., Hindsley, R. B., Hennessy, G. S., Kent, S. M., Lupton, R. H., & Ivezić, Ž. 2003, *AJ*, 125, 1559
- Postman, M. & Lauer, T. R. 1995, *ApJ*, 440, 28
- Quintero, A. D. et al. 2004, *ApJ*, 602, 190
- Roberts, M. S. & Haynes, M. P. 1994, *ARA&A*, 32, 115
- Rudnick, G., Labbé, I., Förster Schreiber, N. M., Wuyts, S., Franx, M., Finlator, K., Kriek, M., Moorwood, A., Rix, H.-W., Röttgering, H., Trujillo, I., van der Wel, A., van der Werf, P., & van Dokkum, P. G. 2006, *ApJ*, 650, 624
- Sandage, A. 1972, *ApJ*, 178, 1
- Schlegel, D. J., Finkbeiner, D. P., & Davis, M. 1998, *ApJ*, 500, 525
- Schneider, D. P., Gunn, J. E., & Hoessel, J. G. 1983, *ApJ*, 264, 337
- Scoccamarro, R., Sheth, R. K., Hui, L., & Jain, B. 2001, *ApJ*, 546, 20

- Smith, B. J., Struck, C., Hancock, M., Appleton, P. N., Charmandaris, V., & Reach, W. T. 2007, *AJ*, 133, 791
- Smith, J. A., Tucker, D. L., et al. 2002, *AJ*, 123, 2121
- Stoughton, C. et al. 2002, *AJ*, 123, 485
- Strateva, I. et al. 2001, *AJ*, 122, 1861
- Strauss, M. A. et al. 2002, *AJ*, 124, 1810
- Toomre, A. 1977, in *Evolution of Galaxies and Stellar Populations*, 401–+
- Tucker, D. L. et al. 2006, *Astronomische Nachrichten*, 327, 821
- van Dokkum, P. G. 2005, *AJ*, 130, 2647
- van Dokkum, P. G., Franx, M., Fabricant, D., Kelson, D. D., & Illingworth, G. D. 1999, *ApJ*, 520, L95
- Wake, D. A. et al. 2006, *MNRAS*, 372, 537
- Willmer, C. N. A. et al. 2005, *ApJ*, submitted, (astro-ph/0506041)
- Zehavi, I., Eisenstein, D. J., Nichol, R. C., Blanton, M. R., Hogg, D. W., Brinkmann, J., Loveday, J., Meiksin, A., Schneider, D. P., & Tegmark, M. 2005, *ApJ*, 621, 22

Fractional luminosity growth of LRGs from mergers

$[M_{0.3i} - 5 \log_{10} h]$ [mag]	Red max [ $10^{-3} \text{ Gyr}^{-1}$ ]	Blue max [ $10^{-3} \text{ Gyr}^{-1}$ ]	Red DF [ $10^{-4} \text{ Gyr}^{-1}$ ]	Blue DF [ $10^{-4} \text{ Gyr}^{-1}$ ]
–24.00 to –23.22	$0.59 \pm 0.31$	$0.35 \pm 0.52$	$1.72 \pm 0.89$	$1.01 \pm 1.52$
–23.22 to –22.53	$1.49 \pm 0.36$	$0.02 \pm 0.33$	$8.53 \pm 2.08$	$0.12 \pm 1.88$
–22.53 to –21.92	$4.22 \pm 0.38$	$0.05 \pm 0.23$	$40.6 \pm 3.65$	$0.53 \pm 2.20$
–21.92 to –21.39	$6.34 \pm 0.32$	$0.88 \pm 0.21$	$36.1 \pm 1.80$	$5.01 \pm 1.19$
–21.39 to –20.92	$7.01 \pm 0.28$	$0.94 \pm 0.14$	$25.2 \pm 1.01$	$3.39 \pm 0.51$
–20.92 to –20.51	$6.46 \pm 0.20$	$1.27 \pm 0.12$	$15.5 \pm 0.47$	$3.05 \pm 0.30$
–20.51 to –20.15	$5.90 \pm 0.17$	$1.16 \pm 0.10$	$9.91 \pm 0.28$	$1.94 \pm 0.17$
–20.15 to –19.83	$4.43 \pm 0.12$	$1.12 \pm 0.09$	$5.45 \pm 0.14$	$1.38 \pm 0.11$
–19.83 to –19.55	$2.96 \pm 0.08$	$1.17 \pm 0.07$	$2.76 \pm 0.08$	$1.09 \pm 0.07$
–19.55 to –19.30	$2.10 \pm 0.07$	$0.92 \pm 0.06$	$1.54 \pm 0.05$	$0.68 \pm 0.05$
–19.30 to –19.09	$1.36 \pm 0.06$	$0.86 \pm 0.05$	$0.81 \pm 0.03$	$0.51 \pm 0.03$
–19.09 to –18.89	$0.85 \pm 0.04$	$0.66 \pm 0.04$	$0.42 \pm 0.02$	$0.32 \pm 0.02$
–18.89 to –18.73	$0.54 \pm 0.03$	$0.42 \pm 0.03$	$0.22 \pm 0.01$	$0.17 \pm 0.01$
–18.73 to –18.58	$0.36 \pm 0.02$	$0.31 \pm 0.03$	$0.13 \pm 0.01$	$0.11 \pm 0.01$
–18.58 to –18.45	$0.21 \pm 0.02$	$0.21 \pm 0.02$	$.066 \pm .005$	$.068 \pm .006$
–18.45 to –18.34	$0.13 \pm 0.01$	$0.15 \pm 0.02$	$.037 \pm .004$	$.042 \pm .006$
–18.34 to –18.23	$0.08 \pm 0.01$	$0.09 \pm 0.01$	$.020 \pm .003$	$.023 \pm .003$
–18.23 to –18.15	$.058 \pm .008$	$.073 \pm .012$	$.014 \pm .002$	$.017 \pm .003$
–18.15 to –18.07	$.025 \pm .006$	$.056 \pm .008$	$.005 \pm .001$	$.012 \pm .002$
–18.07 to –18.00	$.023 \pm .005$	$.041 \pm .009$	$.005 \pm .001$	$.008 \pm .002$

Table 1: Measurements of the fractional growth of spectroscopic LRGs over a Gyr through merger events with different imaging subsamples of companion galaxies with different magnitude ranges and colors. The second and third (“max”) columns present the measurements under the maximal assumption that all pairs merge in an orbital time. The fourth and fifth (“DF”) columns present the measurements under the more realistic dynamical-friction assumption. Note that the “max” and “DF” columns are given in units that differ by a factor of 10.

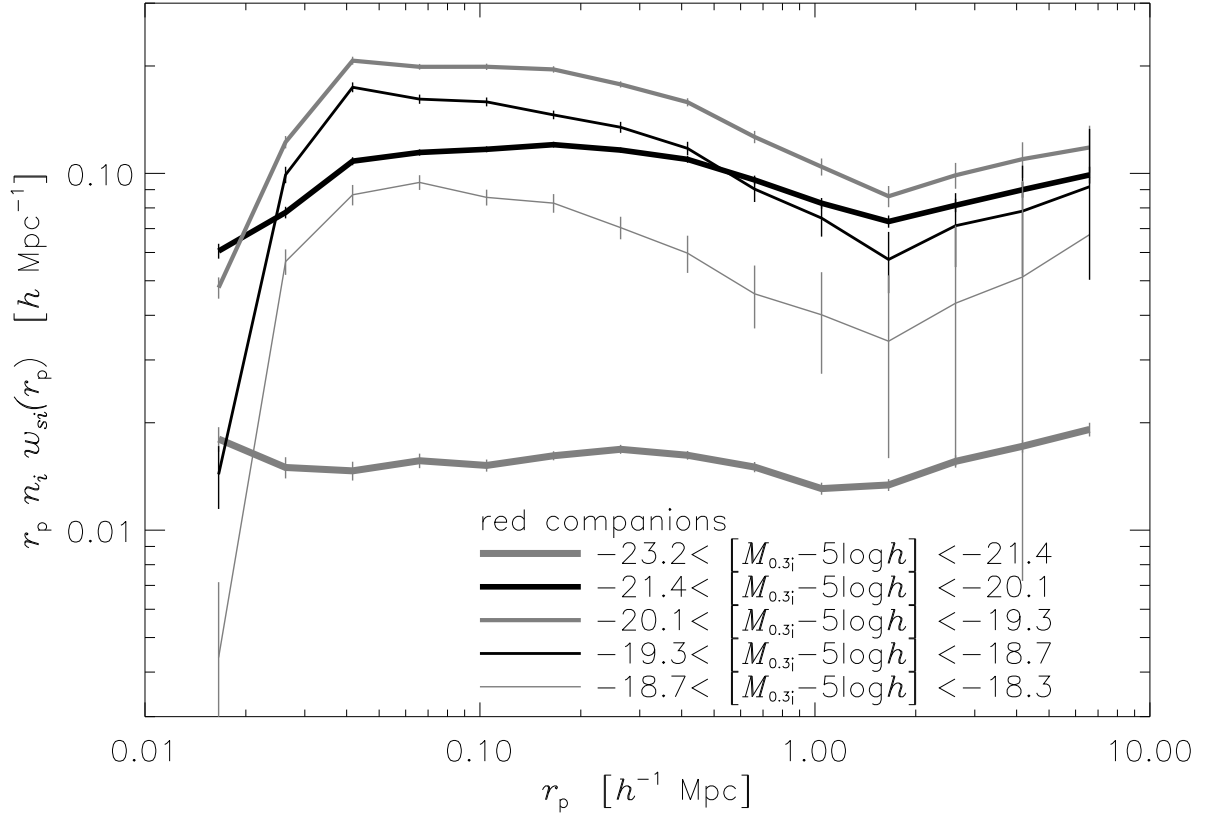


Fig. 1.— Projected two-dimensional cross-correlation functions  $n_i w_{si}(r_p)$  of spectroscopic LRGs  $s$  with *red* companion imaging galaxy subsamples  $i$  with different luminosity ranges, weighted by the number density of each imaging subsample,  $n_i$ , and scaled by  $r_p$  for better illustration. The spectroscopic LRG subsample  $s$  has absolute magnitudes  $-23.2 < [M_{0.3g} - 5 \log_{10} h] < -21.2$  mag and has been trimmed to redshifts  $0.16 < z < 0.30$ . The uncertainties are estimated by jackknife, with jackknife trials dropping contiguous sky regions (see text).

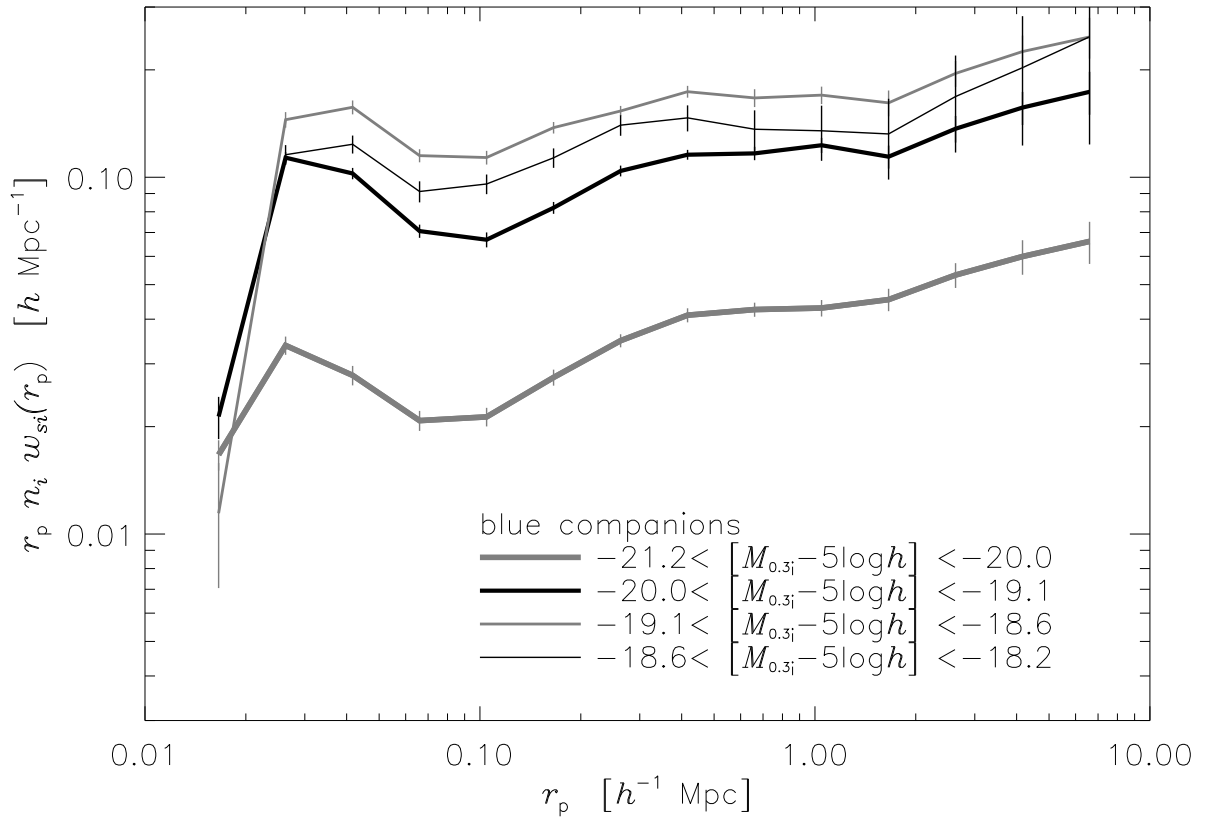


Fig. 2.— Same as Figure 1 but for *blue* companion imaging galaxy subsamples *i*.



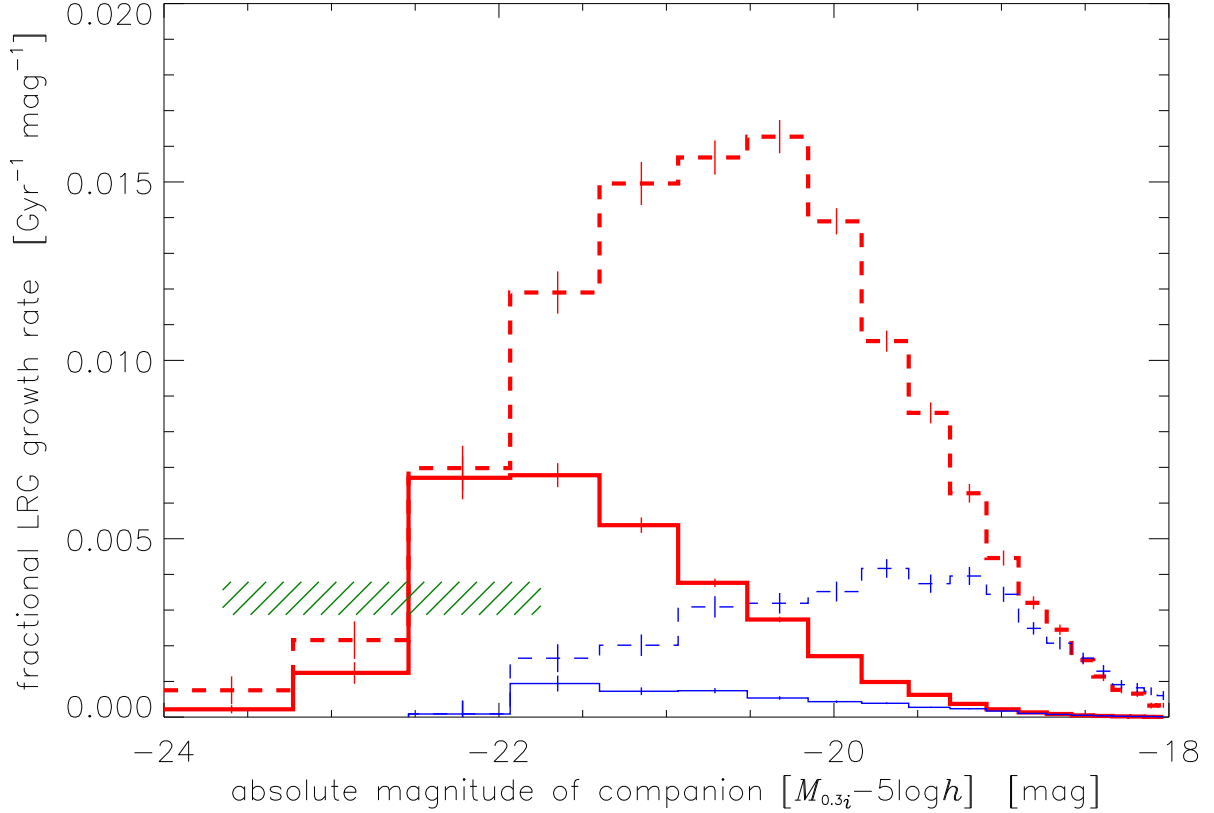


Fig. 3.— The mean fractional luminosity growth of LRGs per Gyr per unit absolute magnitude of the companion, derived from the data in Table 1. The dashed thick red and thin blue lines show this quantity for the red and blue companions respectively, made under the maximal assumption that all companion galaxies merge into the LRG in one orbital time. The solid thick red and thin blue lines show the same thing but made under the more realistic assumption that companion galaxies merge in a time governed by dynamical friction. The total fractional growth rate is the integral (area) under the curves. The green hatched region shows the result of our previous work (Masjedi et al. 2006).